

# Merger of black hole–neutron star binaries in full general relativity

Masaru Shibata<sup>1</sup> and Koji Uryū<sup>2</sup>

<sup>1</sup> Graduate School of Arts and Sciences, University of Tokyo, Komaba, Meguro, Tokyo 153-8902, Japan

<sup>2</sup> Department of Physics, University of Wisconsin-Milwaukee, PO Box 413, Milwaukee, WI 53201, USA

Received 14 November 2006, in final form 11 January 2007

Published 30 May 2007

Online at [stacks.iop.org/CQG/24/S125](http://stacks.iop.org/CQG/24/S125)

## Abstract

We present our latest results of simulation for merger of black hole (BH)–neutron star (NS) binaries in full general relativity which is performed preparing a quasicircular state as the initial condition. The BH is modelled by a moving puncture with no spin and the NS by the  $\Gamma$ -law equation of state with  $\Gamma = 2$  and a corotating velocity field as a first step. The mass of the BH is chosen to be  $\approx 3.2M_{\odot}$  or  $4.0M_{\odot}$ , and the rest mass of the NS  $\approx 1.4M_{\odot}$  with a relatively large radius of the NS  $\approx 13$ – $14$  km. The NS is tidally disrupted near the innermost stable orbit, but  $\sim 80$ – $90\%$  of the material is swallowed into the BH and the resulting disc mass is not very large as  $\sim 0.3M_{\odot}$  even for a small BH mass  $\sim 3.2M_{\odot}$ . The result indicates that the system composed of BH and a massive disc of  $\sim M_{\odot}$  is not formed from nonspinning BH–NS binaries irrespective of the BH mass, although a disc of mass  $\sim 0.1M_{\odot}$  is a possible outcome for this relatively small BH mass range as  $\sim 3$ – $4M_{\odot}$ . Our results indicate that the merger of low-mass BH and NS may form a central engine of short-gamma-ray bursts.

PACS numbers: 04.25.Dm, 04.60.–w, 04.40.Dg

(Some figures in this article are in colour only in the electronic version)

## 1. Introduction

Merger of black hole (BH)–neutron star (NS) binaries is one of the most likely sources for kilometre size laser interferometric gravitational wave detectors. Although such a system has not been observed yet in contrast to NS–NS binaries, statistical studies based on the stellar evolution synthesis suggest that the merger will happen more than 10% as frequently as the merger of binary NSs [1, 2]. Thus, the detection of such a system will be achieved by laser

interferometers in the near future. This motivates theoretical studies for the merger of BH–NS binaries.

According to a study based on the tidal approximation (which is referred to as a study of the configuration of a Newtonian star in circular orbits around a BH in its relativistic tidal field; see, e.g., [3–7]), the fate is classified into two cases, depending on the mass ratio  $q \equiv M_{\text{NS}}/M_{\text{BH}}$ , where  $M_{\text{BH}}$  and  $M_{\text{NS}}$  denote the masses of BH and NS, respectively. For  $q \lesssim q_c$ , the NS of radius  $R$  will be swallowed into the BH horizon without tidal disruption before the orbit reaches the innermost stable circular orbit (ISCO) [5, 6]. On the other hand, for  $q \gtrsim q_c$ , the NS will be tidally disrupted before plunging into the BH. Here, the critical value of  $q_c$  depends on the BH spin and the equation of state (EOS) of the NS. For the nonspinning case with stiff EOSs,  $q_c \approx 0.3\text{--}0.35(R/5M_{\text{NS}})^{-3/2}$  and for the case that the spin of the BH aligns with the orbital angular momentum,  $q_c$  can be smaller [6]. (Throughout this paper, we adopt the geometrical units  $c = G = 1$ .)

The tidal disruption has been studied with great interest for the following reasons. (i) Gravitational waves at tidal disruption will bring information about the NS radius since the tidal disruption limit depends sensitively on it [8]. The relation between the mass and the radius of NSs may be used for determining the EOS of high density matter [9]. (ii) Tidally disrupted NSs may form a massive disc of mass  $\sim 0.1\text{--}1M_{\odot}$  around BH if the tidal disruption occurs outside the ISCO. Systems consisting of a rotating BH surrounded by a massive, hot disc have been proposed as one of likely sources for the central engine of gamma-ray bursts (GRBs) with a short duration [10] and, hence, the merger of low-mass BH and NS is a candidate.

However, the scenario based on the tidal approximation studies may be incorrect since gravitational radiation reaction and self-gravitational effects of the NS in the orbital motion are ignored. Radiation reaction shortens the time available for tidally disrupting NSs. The gravity of the NS could increase the orbital radius of the ISCO and hence the critical value of the tidal disruption,  $q_c$ , may be larger in reality. Miller [11] estimates these ignored effects and suggests that NSs of canonical mass and radius will be swallowed into BHs without tidal disruption. Moreover, NSs are described by the Newtonian gravity in the tidal approximation. If we treat it in general relativity, the self-gravity is stronger and hence tidal disruption is less likely.

Tidal disruption of NSs by BHs has been investigated in the Newtonian [12] and approximately general relativistic (GR) simulation [7, 13]. However, the criterion of tidal disruption will depend on GR effects as mentioned above and, hence, a simulation in full general relativity is obviously required (see [14] for an effort). In [15], we present our first numerical results for fully GR simulation, performed by our new code which has been improved from the previous one [16, 17]; we handle an orbiting BH adopting the moving puncture method, which has been recently developed by two groups [18] (see also [19] for a detailed calibration of this method). As the initial condition, we prepare a quasicircular state computed in a new formalism described in section 2. Focusing particularly on whether NSs of realistic mass and radius are tidally disrupted to form a massive disc around nonspinning BHs, we illustrate that a disc with mass  $\sim M_{\odot}$  is an unlikely outcome for plausible values of NS mass and radius and for BH mass greater than  $3M_{\odot}$ , although a disc of mass of  $O(0.1M_{\odot})$  is possible.

In this paper, we extend a previous study; we perform a simulation for different BH mass from that in [15] to find the dependence of the disc mass on the BH mass. In addition, gravitational waveforms are computed. The paper is organized as follows. In section 2, we describe a formulation for computing quasicircular states in the moving-puncture framework. Section 3 presents some of numerical results for the quasicircular orbits. In section 4, we report numerical results of simulations for the merger of BH–NS binaries. Section 5 is devoted to a summary and discussion.

## 2. Formalism for a quasicircular state

Three groups have worked in computing quasicircular states of BH–NS binaries [20–22]. However, this field is still in an early stage in contrast to computation for NS–NS binaries (e.g., [23]). In [15], we proposed a new method for computing accurate quasicircular states that can be used for numerical simulation in the moving-puncture framework [18, 24]. Here, we briefly describe the formulation.

Even just before the merger, it is acceptable to assume that BH–NS binaries are in a quasicircular orbit since the time scale of gravitational radiation reaction is a few times longer than the orbital period. Thus, we assume the presence of a helical Killing vector around the mass centre of the system,  $\ell^\mu = (\partial_t)^\mu + \Omega(\partial_\varphi)^\mu$ , where the orbital angular velocity  $\Omega$  is constant.

In the present work, we assume that the NS is corotating around the mass centre of the system for simplicity (the definition of mass centre adopted in this formalism is given after equation (5)). An irrotational velocity field is believed to be more realistic for BH–NS binaries [25]. The work for the irrotational case will be reported in a future paper [26]. The assumption of a corotating velocity field in the helical symmetric spacetime yields the first integral of the Euler equation,  $h^{-1}u^t = \text{const}$ , where  $h$  is specific enthalpy defined by  $1 + \varepsilon + P/\rho$ , and  $\varepsilon$ ,  $P$  and  $\rho$  are specific internal energy, pressure and rest-mass density, respectively. In the present work, we adopt the  $\Gamma$ -law EOS with  $\Gamma = 2$ ,  $P = \rho\varepsilon = \kappa\rho^2$  with  $\kappa$  an adiabatic constant.  $u^\mu$  denotes the 4-velocity and  $u^t$  its time component. Assumption of corotation implies  $u^\mu = u^t \ell^\mu$  and thus  $u^r = u^\theta = 0$ .

For a solution of geometric variables of quasicircular orbits, we adopt the conformal flatness formalism for 3-geometry. In this formalism, the solution is obtained by solving Hamiltonian and momentum constraint equations, and an equation for the time slicing condition which is derived from  $K_k^k = 0$  where  $K_{ij}$  is the extrinsic curvature and  $K_k^k$  its trace [27]. Using the conformal factor  $\psi$ , the rescaled tracefree extrinsic curvature  $\hat{A}_i^j \equiv \psi^6 K_i^j$ , and weighted lapse  $\Phi \equiv \alpha\psi$  where  $\alpha$  is the lapse function, these equations are respectively written as

$$\Delta\psi = -2\pi\rho_H\psi^5 - \frac{1}{8}\hat{A}_i^j\hat{A}_j^i\psi^{-7}, \quad (1)$$

$$\hat{A}_{i,j}^j = 8\pi J_i\psi^6, \quad (2)$$

$$\Delta\Phi = 2\pi\Phi \left[ \psi^4(\rho_H + 2S) + \frac{7}{16\pi}\psi^{-8}\hat{A}_i^j\hat{A}_j^i \right], \quad (3)$$

where  $\Delta$  denotes the flat Laplacian,  $\rho_H = \rho h(\alpha u^t)^2 - P$ ,  $J_i = \rho h \alpha u^t u_i$  and  $S = \rho h[(\alpha u^t)^2 - 1] + 3P$ .

We solve these equations in the framework of the puncture BH [18, 24, 28]. Assuming that the puncture is located at  $r_p$ , we set  $\psi$  and  $\Phi$ :

$$\psi = 1 + \frac{M_p}{2r_{\text{BH}}} + \phi \quad \text{and} \quad \Phi = 1 - \frac{C}{r_{\text{BH}}} + \eta, \quad (4)$$

where  $M_p$  and  $C$  are positive constants, and  $r_{\text{BH}} = |x_{\text{BH}}^k|$  ( $x_{\text{BH}}^k = x^k - x_p^k$ ). Then elliptic equations for functions  $\phi$  and  $\eta$  are derived. The constant  $M_p$  is arbitrarily given, while  $C$  is determined from the virial relation (e.g., [29])

$$\oint_{r \rightarrow \infty} \partial_i \Phi dS^i = - \oint_{r \rightarrow \infty} \partial_i \psi dS^i = 2\pi M, \quad (5)$$

where  $M$  is the ADM mass. The mass centre is determined from the condition that the dipole part of  $\psi$  at spatial infinity is zero. In this method, the region with  $\alpha < 0$  exists. However, this does not cause any pathology in the initial value problem.

Equation (2) is rewritten setting

$$\hat{A}_{ij} (= \hat{A}_i^k \delta_{jk}) = W_{i,j} + W_{j,i} - \frac{2}{3} \delta_{ij} \delta^{kl} W_{k,l} + K_{ij}^P, \quad (6)$$

where  $K_{ij}^P$  denotes the weighted extrinsic curvature associated with linear momentum of a puncture BH,

$$K_{ij}^P = \frac{3}{2r_{\text{BH}}^2} (n_i P_j + n_j P_i + (n_i n_j - \delta_{ij}) P_k n_k). \quad (7)$$

Here,  $n^k = n_k = x_{\text{BH}}^k / r_{\text{BH}}$ .  $P_i$  denotes linear momentum of the BH, determined from the condition that the total linear momentum of the system should be zero;

$$P_i = - \int J_i \psi^6 d^3x. \quad (8)$$

The RHS of equation (8) denotes the total linear momentum of the companion NS. Then, the total angular momentum of the system is derived from

$$J = \int J_\varphi \psi^6 d^3x + \epsilon_{zjk} r_{\text{P}}^j \delta^{kl} P_l. \quad (9)$$

The elliptic equation for  $W_i (= W^i)$  is

$$\Delta W_i + \frac{1}{3} \partial_i \partial_k W^k = 8\pi J_i \psi^6. \quad (10)$$

Denoting  $W_i = 7B_i - (\chi_{,i} + B_{k,i} x^k)$  where  $\chi$  and  $B_i$  are auxiliary functions [30], equation (10) is decomposed into two linear elliptic equations

$$\Delta B_i = \pi J_i \psi^6 \quad \text{and} \quad \Delta \chi = -\pi J_i x^i \psi^6. \quad (11)$$

Computing BH–NS binaries in a quasicircular orbit requires determination of the shift vector even in the puncture framework. This is because  $u_i$  has to be obtained (it is derived from  $u_k = \delta_{ki} u^t \psi^4 (v^i + \beta^i)$ , where  $v^i = \Omega \varphi^i$ ). The relation between  $\beta^i$  and  $\hat{A}_{ij}$  is written

$$\delta_{jk} \partial_i \beta^k + \delta_{ik} \partial_j \beta^k - \frac{2}{3} \delta_{ij} \partial_k \beta^k = \frac{2\alpha}{\psi^6} \hat{A}_{ij}. \quad (12)$$

Operating  $\delta^{jl} \partial_l$ , an elliptic equation is derived

$$\Delta \beta^i + \frac{1}{3} \delta^{ik} \partial_k \partial_j \beta^j = 2\partial_j (\alpha \psi^{-6}) \hat{A}^{ij} + 16\pi \alpha J_j \delta^{ij}. \quad (13)$$

Here for  $\hat{A}_{ij}$ , we substitute the relation of equation (6) (not equation (12)). As a result, no singular term appears on the RHS of equation (13), and equation (13) is solved in the same manner as that for  $W_i$ .

We have computed several models of quasicircular states and found that the relation between  $\Omega$  and  $J$  approximately agrees with the third post-Newtonian relation [31]. This confirms that this approach is a fair way to prepare quasicircular states. We also found that in this method, the shift vector at  $\mathbf{r} = \mathbf{r}_{\text{P}}$  automatically satisfies the condition  $\beta^\varphi = -\Omega$  within the error of a few per cent. This implies that the puncture is approximately guaranteed to be in a corotating orbit in the solution.

**Table 1.** Parameters of quasicircular states. Mass parameter of puncture, mass of BH, rest mass of NS, mass, radius and normalized mass of NS in isolation, total mass of the system, nondimensional angular momentum parameter, orbital period in units of  $M$  and compactness of the system defined by  $C_o = (M\Omega)^{2/3}$ . The mass of BH is computed from the area of the apparent horizon  $A$  as  $(A/16\pi)^{1/2}$ . The mass is shown in units of  $M_\odot$ .

	$M_P$	$M_{\text{BH}}$	$M_*$	$M_{\text{ONS}}$	$R$ (km)	$M_*/\kappa^{1/2}$	$M$	$J/M^2$	$P_0/M$	$C_o$
A	3.13	3.21	1.40	1.30	13.8	0.147	4.47	0.729	119	0.141
B	3.13	3.21	1.40	1.30	13.8	0.147	4.47	0.720	110	0.150
C	3.93	4.01	1.40	1.30	13.0	0.151	5.26	0.645	115	0.144

### 3. Numerical results for quasicircular states

BH–NS binaries in quasicircular orbits have been computed for a wide variety of models with  $q = M_*/M_{\text{BH}} \approx 0.3\text{--}0.5$ , where  $M_*$  denotes the baryon rest mass of the NS. In the present work, the compactness of spherical NSs with the rest mass  $M_*$  is chosen to be  $\approx 0.14\text{--}0.15$ . In the  $\Gamma$ -law EOSs, the mass and radius of NS are rescaled by changing the value of  $\kappa$ . In the following, we fix the unit by setting that  $M_* = 1.4M_\odot$ .

In computation, we focus only on the orbit slightly outside the ISCO. In table 1, we show the quantities for selected quasicircular states with  $q \approx 0.4$  and  $0.33$ . For models A and B shown in table 1, the radius of NS in isolation is  $R \approx 13.8$  km, the gravitational mass in isolation is  $M_{\text{ONS}} \approx 1.30M_\odot$  and  $M_*/\kappa^{1/2} = 0.147$ . For model C,  $R \approx 13.0$  km,  $M_{\text{ONS}} \approx 1.3M_\odot$  and  $M_*/\kappa^{1/2} = 0.151$ . According to theories for NSs based on realistic nuclear EOSs [32], the radius of a NS of  $M_{\text{NS}} \approx 1.4M_\odot$  is 11–13 km. Thus, the radius chosen here is slightly larger than that of realistic NSs and is more subject to tidal disruption. Model A is that used for the following numerical simulation and model B is very close to the tidal disruption limit of approximately the same mass as that of model A, showing that the model A has an orbit slightly outside the tidal disruption limit. This is also the case for model C. As we show in the following section, tidal disruption sets in after a small decrease of orbital separation for models A and C.

The tidal approximation studies suggest that for  $q \gtrsim q_*$ , NSs could be tidally disrupted by BHs [6]. Here, in the tidal approximation, the critical value  $q_*$  for  $\Gamma = 2$  and for nonspinning BHs is approximately given by

$$q_* \equiv 0.35 \left( \frac{R}{5M_{\text{NS}}} \right)^{-3/2} \frac{(M_{\text{BH}}\Omega)^{-1}}{6^{3/2}}, \quad (14)$$

and  $\Omega = M_{\text{BH}}^{-1}/6^{3/2}$  is the angular velocity of the ISCO around nonspinning BHs. For models A and B,  $q_* \approx 0.32$  and, hence,  $q > q_*$ . According to the tidal approximation studies [5, 6], such NS should be unstable against tidal disruption. Nevertheless, such equilibrium exists, proving that the tidal disruption limit in the framework of the tidal approximation does not give a correct answer. Our studies indicate that the critical value  $q_*$  is  $\approx 0.43(R/5M_{\text{NS}})^{-3/2}[(M_{\text{BH}}\Omega)^{-1}/6^{3/2}]$ ; the tidal disruption of NS is much less likely than in the prediction by the tidal approximation [5, 6]. For a typical NS of radius  $R \sim 5M_{\text{NS}}$  and mass  $M_{\text{NS}} \sim 1.4M_\odot$ ,  $M_{\text{BH}} \lesssim 3.3M_\odot$  will be necessary for  $(M_{\text{BH}}\Omega)^{-2/3} \geq 6$ ; this implies that canonical NSs will not be tidally disrupted outside the ISCO by most of nonspinning BHs of mass larger than  $\sim 3M_\odot$ . Tidal disruption occurs only for NSs of relatively large radius and only for orbits very close to the ISCO.

In this work, the criterion for the tidal disruption is investigated only for  $\Gamma = 2$  EOS and for compactness 0.14–0.15. The criterion is likely to depend on the stiffness of the EOS [6]

since the structure of NSs depends on it. The criterion should also depend strongly on the compactness of NSs in general relativity which has a nonlinear nature. In the future paper, we plan to determine the criterion for a wide variety of EOSs and compactness of NSs [26].

#### 4. Simulation for merger

Even if tidal disruption of an NS occurs near the ISCO, a massive disc may be formed around the companion BH. To investigate the outcome after merger and resulting gravitational waveforms, we perform numerical simulation adopting models A and C.

For the simulation, we initially reset the lapse (i.e.  $\Phi$ ) since the relation  $\alpha \geq 0$  should hold everywhere. In the present work,  $\Phi$  at  $t = 0$  is given by

$$\Phi = \eta + \frac{1 + 0.1X^4}{1 + \sum_{m=1}^3 X^m + 1.1X^4}, \quad (15)$$

where  $X = C/r_{\text{BH}}$ . Then,  $\alpha = 0$  only at puncture and otherwise  $\alpha > 0$ . Furthermore, for  $r_{\text{BH}} > C$ , the values of  $\Phi$  quickly approach those of the quasicircular states.

The numerical code for hydrodynamics is the same as that for performing merger of NS–NS binaries (a high-resolution central scheme) [17, 33]. On the other hand, we change equations for  $\alpha$ ,  $\beta^i$  and  $\psi$ , and numerical scheme of handling the transport terms of evolution equations for geometries. For  $\alpha$  and  $\beta^i$ , we solve

$$(\partial_t - \beta^i \partial_i) \ln \alpha = -2K_k^k, \quad (16)$$

$$\partial_t \beta^i = 0.75 \tilde{\gamma}^{ij} (F_j + \Delta t \partial_t F_j), \quad (17)$$

where  $\tilde{\gamma}_{ij}$  is the conformal 3-metric and  $F_i = \delta^{jk} \partial_j \tilde{\gamma}_{ik}$ .  $\Delta t$  denotes the time step for the simulation, and the second term on the RHS of equation (17) is introduced for stabilization. The equation for the conformal factor is also changed to

$$\partial_t \psi^{-6} - \partial_i (\psi^{-6} \beta^i) = (\alpha K_k^k - 2\partial_i \beta^i) \psi^{-6}, \quad (18)$$

since  $\psi$  diverges at the puncture [18].

In addition, we have improved the numerical scheme for the transport term of geometric variables  $(\partial_t - \beta^i \partial_i) Q$ , where  $Q$  is one of the geometric variables: First, we rewrite this term as  $\partial_t Q - \partial_i (Q \beta^i) + Q \partial_t \beta^i$  and then apply the same scheme as that in computing the transport term of the hydrodynamic equations to the second term (third-order piece-wise parabolic interpolation scheme [16]). We have found that for evolving BHs, such a high-resolution scheme for the transport term in the geometric variables is crucial. This is probably because of the fact that near punctures, some of geometric variables steeply vary and so does the term  $\beta^i \partial_i Q$ . For other terms in Einstein's equation, we use the second-order finite differencing as in [16, 17]. (Note that in the case of a nonuniform grid, 4-point finite differencing is adopted for  $Q_{,ii}$  since the 3-point one is first order.) After we performed most of runs, we iterated some of the computations with a third-order scheme (5-point finite differencing for  $Q_{,ii}$ ) which is used in [18, 19]. We find that with such a scheme, convergent results are obtained with a relatively large grid spacing. However, the results are qualitatively unchanged and the extrapolated results (which are obtained in the limit of zero grid spacing; see below) are approximately identical.

In the simulation, the cell-centred Cartesian,  $(x, y, z)$ , grid is adopted to avoid the situation that the location of punctures (which always stay in the  $z = 0$  plane) coincides with the grid location. The equatorial plane symmetry is assumed and the grid size is  $(2N, 2N, N)$  for  $x$ – $y$ – $z$ , where  $N$  is a constant. Following [34], we adopt a nonuniform grid; in the present

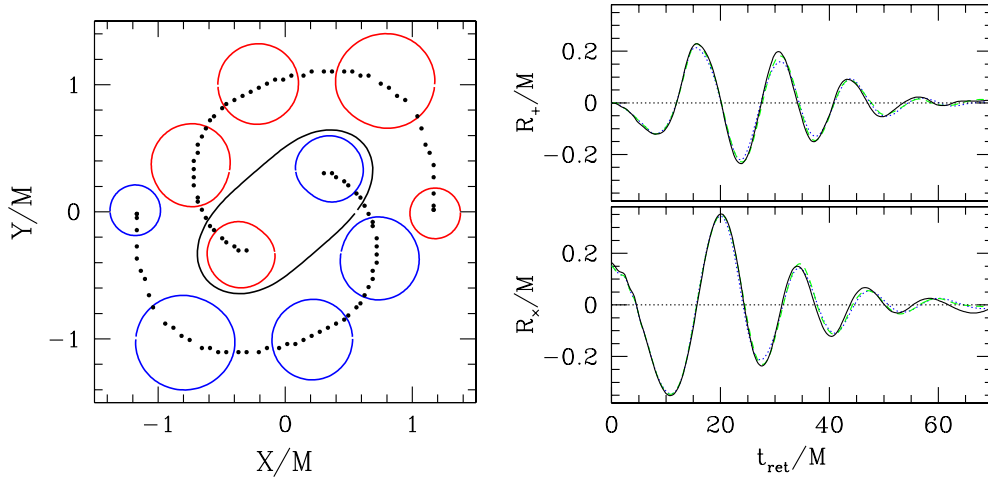


**Figure 1.** Numerical results for merger of binary BHs performed with the initial data of [18]. Left: the open-thick circles denote the locations of the apparent horizon of two BHs for  $t/M = 0, 5, 10, 15$  and  $20$ , where  $M$  is the total ADM mass at  $t = 0$ . The open-wide circle at  $t = 20M$  is the common apparent horizon. The small-solid dots denote the locations of the maximum of the conformal factor. The grid setting is  $(N, N_0, \Delta i, \xi, \Delta x/M_p, L/\lambda) = (200, 105, 30, 7, 1/16, 1.20)$  for this result (note that  $\lambda \approx 37M$ ). Right: + and  $\times$  modes of gravitational waveforms extracted at  $r \approx \lambda$  for  $(N, N_0, \Delta i, \xi, \Delta x/M_p, L/\lambda) = (200, 105, 30, 9, 0.05, 1.20)$  (solid curves),  $(200, 105, 30, 7, 0.064, 1.23)$  (dashed curves) and  $(200, 105, 30, 5, 0.08, 1.23)$  (dotted curves).

approach, a domain of  $(2N_0, 2N_0, N_0)$  grid zone is covered with a uniform grid of spacing  $\Delta x$  and outside the domain, the grid spacing is increased according to  $\xi \tanh[(i - N_0)/\Delta i]\Delta x$ , where  $i$  denotes the  $i$ th grid point in each direction.  $N_0, \Delta i$  and  $\xi$  are constants. For model A,  $\Delta x/M_p$  is chosen to be  $10/80, 9/80, 8/80, 7/80$  and  $6/80$ , and for model C, it is  $7/120, 8/120, 9/120$  and  $10/120$ . Campanelli *et al* [18] suggest that such grid spacing can resolve moving punctures. For model A,  $(N, N_0, \Delta i, \xi, \Delta x/M_p, L/\lambda)$  is chosen to be  $(160, 105, 30, 4.5, 10/80, 0.46)$ ,  $(200, 105, 30, 4.5, 10/80, 0.78)$ ,  $(200, 105, 30, 5, 10/80, 0.83)$ ,  $(220, 125, 30, 5, 9/80, 0.78)$ ,  $(220, 125, 30, 6, 8/80, 0.78)$ ,  $(220, 140, 30, 7, 7/80, 0.65)$  and  $(220, 150, 9, 6/80, 0.59)$ . Here,  $L$  and  $\lambda$  denote the location of the outer boundaries along each axis and the wavelength of gravitational waves at  $t = 0$ . For model A with  $\Delta x = M_p/8$  and  $N = 160$ , we chose other values of  $N_0$  and  $\Delta i$ , and found that the results very weakly depend on them as well as on  $L$  as far as  $L \gtrsim \lambda/2$ . For model C, the chosen parameters are  $(200, 120, 30, 6, 1/12, 0.53)$ ,  $(220, 125, 30, 6, 9/120, 0.58)$ ,  $(220, 125, 30, 7, 8/120, 0.58)$  and  $(220, 140, 30, 8, 7/120, 0.48)$ . For all cases, numerical computations were performed throughout the merger until the accretion rate of the matter onto BH relaxes to approximately constant.

For a test, we performed simulations for the merger of two nonspinning BHs adopting the same initial condition as used in [18]. We focused particularly on the merger time, which is referred to as the time at which a common apparent horizon is first formed and found that it varies with improving grid resolution approximately at first order. The likely reason is that geometric variables vary steeply around the BH where they are evolved with first-order accuracy in our scheme, although other regions are resolved with second-order accuracy. By extrapolation, an exact merger time is estimated to be  $\approx 19M$ . This result agrees approximately with that of [18]. This indicates that our code can follow moving punctures (see the left panel of figure 1 for evolution of the location of apparent horizons for the initial condition of [18]).

Gravitational waves are also computed using a gauge-invariant extraction method used in [16, 17, 34]. In the right panel of figure 1, we display the results for three different

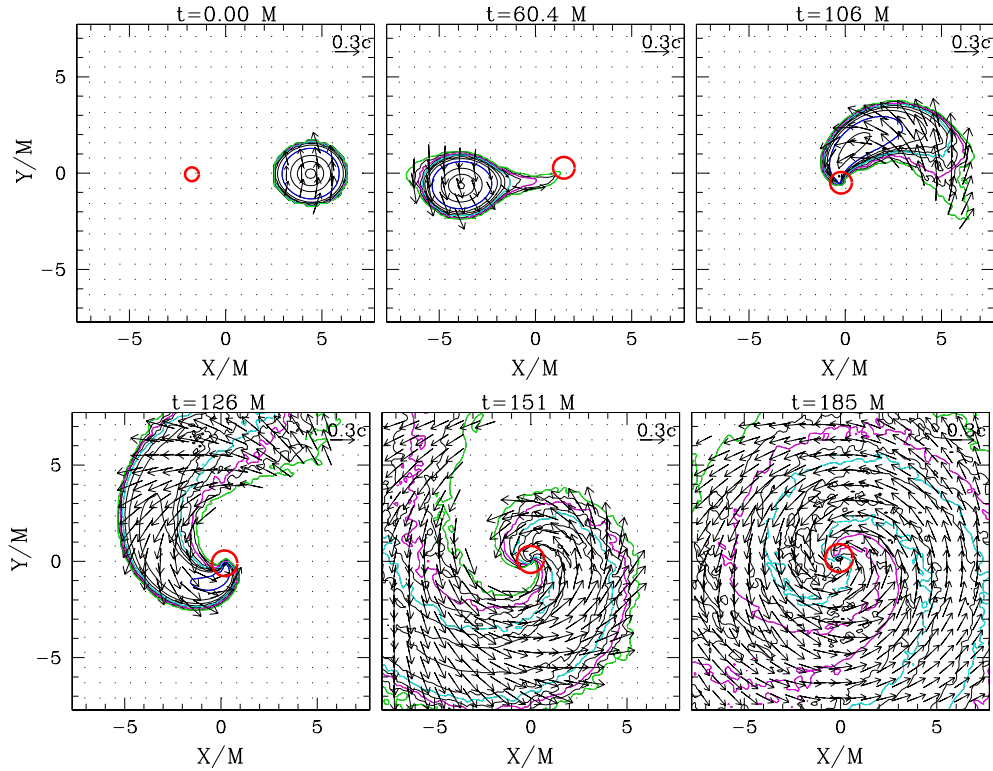


**Figure 2.** Snapshots of the density contour curves for  $\rho$  in the equatorial plane for model A with  $(N, N_0, \Delta i, \xi, \Delta x/M_p, L/\lambda) = (220, 150, 9, 3/40, 0.59)$ . The solid contour curves are drawn for  $\rho = (1 + 2i) \times 10^{14} \text{ g cm}^{-3}$  ( $i = 1, 2, 3$ ) and for  $10^{14-0.5i} \text{ g cm}^{-3}$  ( $i = 1-8$ ). The maximum density at  $t = 0$  is  $\approx 7.2 \times 10^{14} \text{ g cm}^{-3}$ . (In the Web version, the blue, cyan, magenta and green curves denote  $10^{14}$ ,  $10^{12}$ ,  $10^{11}$  and  $10^{10} \text{ g cm}^{-3}$ , respectively). The vectors indicate the velocity field  $(v^x, v^y)$ , and the scale is shown in the upper right-hand corner. The thick (red) circles are apparent horizons. Time is shown in units of total mass of the system  $M$ .

grid resolutions. The figure shows that after merger, gravitational waves are determined by the quasinormal mode ringing and that the waveforms depend very weakly for chosen grid resolutions. The wavelength of the quasinormal mode is  $\approx 11-12M$ , which agrees with the result of [18].

Next, we present the results for model A. Figure 2 shows the evolution of contour curves for  $\rho$  and velocity vectors for  $v^i$  in the equatorial plane together with the location of apparent horizons at selected time slices for  $(N, N_0, \Delta i, \xi, \Delta x/M_p, L/\lambda) = (220, 150, 9, 3/40, 0.59)$ . Due to the gravitational radiation reaction, the orbital radius decreases and then the NS is elongated (second panel). Because of the elongation, the quadrupole moment of the NS is amplified and the attractive force between two objects is strengthened [35]. This effect accelerates an inward motion, and consequently the NS starts plunging into the BH at  $t \sim 90M$ . Soon after this time, the NS is tidally disrupted, but the tidal disruption occurs near the ISCO and hence the material in the inner part is quickly swallowed into the BH (third and fourth panels). On the other hand, because of the outward angular momentum transfer, the material in the outer part of the NS forms a disc with the maximum density  $\sim 10^{12} \text{ g cm}^{-3}$  (fifth and sixth panels).

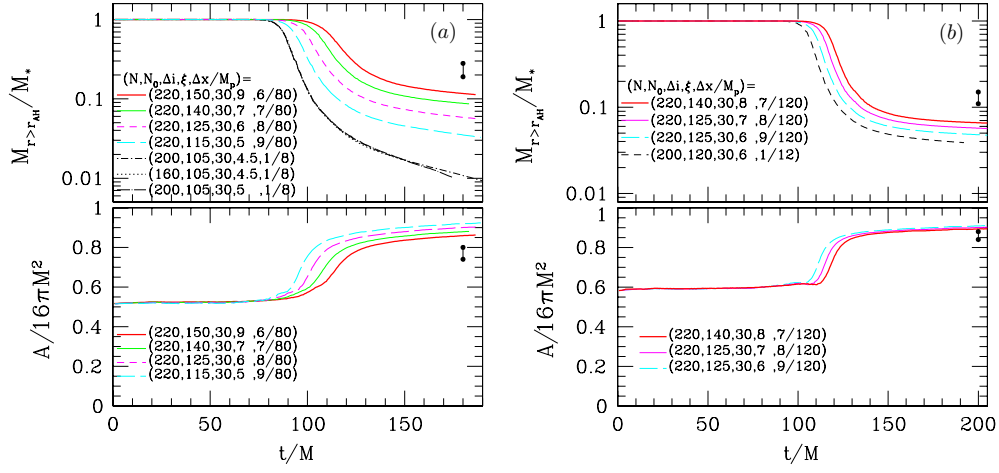


**Figure 3.** (a) Results for model A for various grid resolutions. The upper panel shows evolution of baryon rest mass located outside the apparent horizon. The plots for  $\Delta x = M_p/8$  almost coincide and show that the results depend weakly on the values of  $L$  and  $\xi$ . On the other hand, the results depend systematically on  $\Delta x$  (see the text). The lower panel shows evolution of area of apparent horizon in units of  $16\pi M^2$ . (b) The same as (a) but for model C.

The mass of the disc surrounding the BH formed after the merger is not large. Figure 3(a) shows the evolution of baryon rest mass located outside apparent horizons  $M_{r>r_{\text{AH}}}$ . We find that  $\sim 80\%$  and  $\sim 90\%$  of the mass are swallowed into the BH in  $t \sim 130M \sim 2$  ms for models A and C, respectively, for the best grid-resolution simulations. The swallowing continues after this time. Note that since  $M_{r>r_{\text{AH}}}$  is rest mass outside apparent horizons, the disc mass which should be defined for the mass located outside an ISCO around the formed BH is slightly smaller. We follow the evolution of the rest mass of material located for  $r > 3M$  and  $r > 4.5M$ , where  $r = 3M-4.5M$  are approximate locations of the ISCO around the formed BH, and find that their values are smaller than  $M_{r>r_{\text{AH}}}$  by  $\sim 10\%$  and  $20\%$ , respectively. Thus, the disc mass would be  $0.8-0.9M_{r>r_{\text{AH}}}$  in reality.

The value of  $M_{r>r_{\text{AH}}}$  depends systematically on  $\Delta x$ ; we find that the results for good resolutions ( $\Delta x/M_p = 3/40, 7/80$  and  $1/10$  for model A and  $7/120, 8/120$  and  $9/120$  for model C) at late times approximately obey a relation of convergence, i.e.  $M_{r>r_{\text{AH}}}(t) = a(t) + b(t)\Delta x^n$ , where  $a(t)$  and  $b(t)$  are functions of time. The order of convergence, denoted by  $n$ , is between first and second orders (i.e.  $1 < n < 2$ ). For model A, least-square fitting gives  $a(t)$  at  $t = 180M$  as  $\approx 0.19M_*$  if we set  $n = 2$  and as  $0.28M_*$  for  $n = 1$  (see the solid circles in figure 3(a)). For model C, they are  $0.11M_*$  and  $0.15M_*$  (the solid circles in figure 3(b)), respectively. Thus, the true result should be between  $0.19M_*$  and  $0.28M_*$  for model A and between  $0.11M_*$  and  $0.15M_*$  for model C.

It is reasonable that the disc mass for model C is smaller than for model A since the mass ratio of NS to BH is smaller for model C while the compactness of NS is nearly identical. A remarkable point is that with a small increase of the BH mass from  $3.2M_\odot$  to  $4.0M_\odot$ , the disc mass decreases by a factor of 2. This suggests that the disc mass depends sensitively on the BH mass.

Note that the adopted NS has a corotating velocity field initially, and furthermore its radius is larger than that of canonical NSs. For an irrotational velocity field with a realistic value of radius, the disc mass would be smaller than this value. It is reasonable to consider that our results for the disc mass provide an upper limit of the disc mass for a given mass and

spin of BH. Hence it is unlikely that a massive disc with  $\sim M_\odot$  is formed after the merger of a nonspinning BH of mass  $M > 3M_\odot$  and a canonical NS of mass  $\approx 1.4M_\odot$  and radius  $\approx 11\text{--}13$  km, although a disc of mass of  $\sim 0.2\text{--}0.3M_\odot$  may be formed for a small BH mass ( $\lesssim 4M_\odot$ ). This value of the disc mass is large enough to explain short GRBs of relatively low total energy  $\sim 10^{49}$  ergs (see, e.g., [36] for an estimate).

The lower panels of figure 3 show the evolution of the area of apparent horizons in units of  $16\pi M^2$ . These illustrate that the area of BHs quickly increases on swallowing material, and then the area settles down to an approximate constant. We, again, evaluate the true final area by extrapolation for results with different grid resolutions. For model A, the area in units of  $16\pi M^2$  at  $t = 180M$  is 0.74 and 0.80 in the assumption of the first- ( $n = 1$ ) and second-order ( $n = 2$ ) convergences, respectively (see the solid circles in figure 3(a)). For model C,  $A/16\pi M^2$  at  $t = 200M$  is 0.84 and 0.88 for  $n = 1$  and  $n = 2$ , respectively (see the solid circles in figure 3(b)). From these values the spin parameter of formed BHs,  $a$ , is approximately derived from

$$\frac{A}{16\pi M_{\text{BHf}}^2} = \frac{1 + \sqrt{1 - a^2}}{2}, \quad (19)$$

where  $M_{\text{BHf}}$  denotes the mass of the formed BH. To approximately estimate it, we simply use

$$M_{\text{BHf}} = M - M_{r>r_{\text{AH}}} - E_{\text{GW}}, \quad (20)$$

where  $E_{\text{GW}}$  is energy radiated by gravitational waves. We find that  $E_{\text{GW}}$  is about 1% of  $M$  and simply use relation  $E_{\text{GW}} = 0.01M$ . Then we obtain  $a = 0.57$  and  $0.52$  for  $n = 1$  and  $n = 2$  for model A and  $a = 0.52$  and  $0.42$  for  $n = 1$  and  $n = 2$  for model C, respectively. Thus, spinning BHs of moderate rotation are outcomes.

The spin parameter of the formed BHs is much smaller than the initial value of  $J/M^2$  of the system. One of the reasons is that the disc has large angular momentum approximately written as  $3M_{\text{BHf}}M_{\text{disc}}$ , where  $M_{\text{disc}}$  denotes the disc mass  $\sim 0.8\text{--}0.9M_{r>r_{\text{AH}}}$ . Here, the factor  $3M_{\text{BHf}}$  denotes a value of typical specific angular momentum around the formed BH. Denoting the initial angular momentum by  $a_0M^2$  where  $a_0 \approx 0.73$  and  $0.65$  for models A and C (see table 1), the fraction of angular momentum that the disc has is  $\sim 3a_0^{-1}M_{\text{disc}}M_{\text{BHf}}/M^2$ . Thus, for model A, the fraction is  $\sim 20\text{--}30\%$  and for model C, it is  $10\text{--}15\%$ . In addition, gravitational waves carry away the angular momentum by  $\sim 10\%$  of  $a_0M^2$ . Thus, the angular momentum of the formed BH should be smaller than the initial total angular momentum of the system by  $30\text{--}40\%$  for model A and by  $20\text{--}25\%$  for model C. Therefore, the values for  $a$  derived above are reasonable magnitudes.

In figure 4, gravitational waveforms for model C are shown. Gravitational waves are extracted from the metric near the outer boundaries using a gauge-invariant wave extraction method (see [16, 34] for details). From the values of  $R_+$  and  $R_\times$ , the maximum amplitude of gravitational waves at a distance  $D$  is evaluated

$$h_{\text{gw}} \approx 10^{-22} \left( \frac{\sqrt{R_+^2 + R_\times^2}}{0.31 \text{ km}} \right) \left( \frac{100 \text{ Mpc}}{D} \right). \quad (21)$$

Here, the maximum amplitude can be observed if the observer is located along the  $z$ -axis. Figure 4 implies that the maximum amplitude at a distance of  $D = 100$  Mpc is  $\approx 5 \times 10^{-22}$  since  $M = 5.26M_\odot$ .

For  $t_{\text{ret}} \equiv t - r_{\text{obs}} \lesssim 120M$  ( $r_{\text{obs}}$  is the radius of extracting gravitational waves), inspiral waveforms are seen. The amplitude increases and characteristic wavelength decreases with time. The wavelength at the final phase of the inspiral is  $\sim 25M$  indicating that the orbital

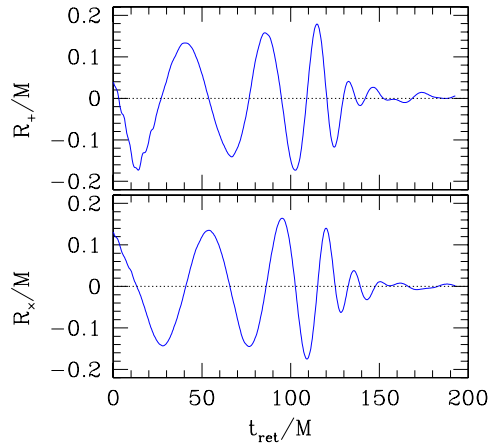


**Figure 4.** + and  $\times$  modes of gravitational waveforms for model C.  $t_{\text{ret}}$  and  $M$  denote the retarded time and the ADM mass of the system, respectively. The amplitude at a distance of an observer can be found from (21).

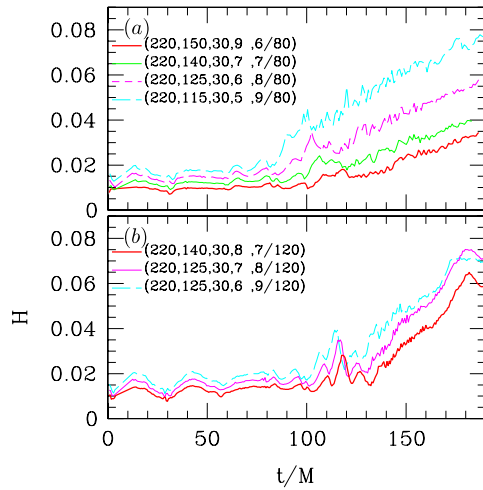


**Figure 5.** Evolution of averaged violation of the Hamiltonian constraint (a) for model A and (b) for model C.

period of the ISCO is  $\sim 50M$  (i.e.  $\Omega \sim 0.12M^{-1}$ ). This is in approximate agreement with the third post-Newtonian results [31].

For  $120M \lesssim t_{\text{ret}} \lesssim 150M$ , ring-down waveforms are seen. The characteristic wavelength is  $\sim 15M_{\text{BHf}}$ , which is in approximate agreement with the wavelength of the quasinormal mode. For  $t_{\text{ret}} \gtrsim 130M$ , the amplitude of gravitational waves damps quickly even during the dynamical formation of a massive disc. This is due to the fact that the degree of nonaxisymmetry of the disc decreases on a very short time scale ( $\sim 20\text{--}30M$ ). This indicates that in the frequency domain, the amplitude of the Fourier power spectrum steeply decreases in the high-frequency region.

Figure 5 shows the evolution of averaged violation of the Hamiltonian constraint. For the average, rest-mass density is used as a weight (see [37] for definition) and the integral is performed for the region outside apparent horizons. The figure shows that the Hamiltonian

constraint converges approximately at second order. This result is consistent with the fact that the region except for the vicinity of the BH is followed with second-order accuracy. As mentioned before, on the other hand, the vicinity of the BH is evolved with first-order accuracy in the present code.

## 5. Discussion

In this paper, we have presented our latest numerical results of fully GR simulation for merger of BH–NS binaries, focusing on the case that the BH is not spinning initially and the mass ratio of NS to BH is fairly large at 0.3–0.4. It is found that even with such high values of the mass ratio, the NS is tidally disrupted only for an orbit very close to the ISCO and 80–90% of the mass element is quickly swallowed into the BH without forming massive discs. The results do not agree quantitatively with the prediction by the tidal approximation study. The reasons are as follows. (1) In the tidal approximation, one describes NSs by Newtonian gravity. In general relativity, gravity is stronger and tidal disruption is less likely. (2) The time scale for angular momentum transfer during tidal disruption near the ISCO is nearly as long as the plunging time scale determined by the gravitational radiation reaction and attractive force between two objects. Hence before the tidal disruption is completed, most of the material is swallowed.

If the BH has a large spin, the final fate may be largely changed because of the presence of the spin–orbit repulsive force. This force can weaken the attractive force between the BH and the NS and slow down the orbital velocity, resulting in smaller gravitational wave luminosity and longer radiation reaction time scale [38]. This effect may help massive disc formation. The study of spinning BH binaries is one of the next issues. The fate will also depend on the EOS of the NS [6] and the mass of the BH as well as on the velocity field of the NS. Simulations with various EOSs and BH mass and with an irrotational velocity field are also next issues.

In this paper, a small number of results for quasicircular states of BH–NS binaries are presented. Currently, we are working on the computation of quasicircular states for a wide variety of masses of BH and NS in the framework described in section 2. The numerical results will be reported in the near future [26].

## Acknowledgments

MS thanks Y Sekiguchi for useful discussions. Numerical computations were performed on the FACOM-VPP5000 at ADAC at NAOJ and on the NEC-SX8 at YITP in Kyoto University. This work was supported in part by Monbukagakusho Grants (no. 17540232) and by NSF grants PHY0071044, 0503366.

## References

- [1] Narayan R, Paczynski B and Piran T 1992 *Astrophys. J.* **395** 83
- [2] Voss R and Taulis T M 2003 *Mon. Not. R. Astron. Soc.* **342** 1169  
Belczynski K, Bulik T and Rudak B 2002 *Astrophys. J.* **571** 394  
Kalogera V *et al* 2004 *Astrophys. J.* **601** L179
- [3] Fishbone L G 1973 *Astrophys. J.* **185** 43  
Mashhoon B 1975 *Astrophys. J.* **197** 705  
Marck J-A 1983 *Proc. R. Soc. Lond. A* **385** 431
- [4] Shibata M 1996 *Prog. Theor. Phys.* **96** 917
- [5] Wiggins P and Lai D 2000 *Astrophys. J.* **532** 530
- [6] Ishii M, Shibata M and Mino Y 2005 *Phys. Rev. D* **71** 044017

- [7] Faber J A, Baumgarte T W, Shapiro S L, Taniguchi K and Rasio F A 2006 *Phys. Rev. D* **73** 024012
- [8] Vallisneri M 2000 *Phys. Rev. Lett.* **84** 3519
- [9] Lindblom L 1992 *Astrophys. J.* **398** 569
- [10] Fryer C L, Woosley S E, Herant M and Davies M B 1999 *Astrophys. J.* **520** 650
- [11] Miller M C 2005 *Astrophys. J.* **626** L41
- [12] Lee W H and Kluzniak W 1999 *Astrophys. J.* **526** 178  
Janka H T, Eberl T, Ruffert M and Fryer C L 1999 *Astrophys. J.* **527** L39  
Rosswog S 2005 *Preprint astro-ph/0505007*
- [13] Faber J A, Baumgarte T W, Shapiro S L and Taniguchi K 2006 *Astrophys. J.* **641** L93
- [14] Löffler F, Rezzolla L and Ansorg M 2006 *Phys. Rev. D* **74** 104018
- [15] Shibata M and Uryū K 2006 *Phys. Rev. D* **74** 121503 (R)
- [16] Shibata M, Taniguchi K and Uryū K 2003 *Phys. Rev. D* **68** 084020
- [17] Shibata M, Taniguchi K and Uryū K 2005 *Phys. Rev. D* **71** 084021  
Shibata M and Taniguchi K 2006 *Phys. Rev. D* **73** 064027
- [18] Campanelli M, Lousto C O, Marronetti P and Zlochower Y 2006 *Phys. Rev. Lett.* **96** 111101  
Baker J G, Centrella J, Choi D-I, Koppitz M and van Meter J 2006 *Phys. Rev. Lett.* **96** 111102  
Herrmann F, Hinder I, Shoemaker D and Laguna P 2007 *Class. Quantum Grav.* **24** S33 (*Preprint gr-qc/0601026*)
- [19] Brügmann B, Conzalez J A, Hannam M, Husa S and Sperhake U 2006 *Preprint gr-qc/0610128*
- [20] Miller M 2001 *Preprint gr-qc/0106017*
- [21] Taniguchi K, Baumgarte T W, Faber J A and Shapiro S L 2006 *Phys. Rev. D* **72** 044008
- [22] Grandclement P 2006 *Preprint gr-qc/0609044*
- [23] Uryū K *et al* 2006 *Phys. Rev. Lett.* **97** 171101
- [24] Brandt S and Brügmann B 1997 *Phys. Rev. Lett.* **78** 3606
- [25] Kochanek C S 1992 *Astrophys. J.* **398** 234  
Bildsten L and Cutler C 1992 *Astrophys. J.* **400** 175
- [26] Uryū K and Shibata M 2007 in preparation
- [27] Wilson J R and Mathews G J 1995 *Phys. Rev. Lett.* **75** 4161
- [28] Hannam M D 2005 *Phys. Rev. D* **72** 044025
- [29] Grandclement P, Gourgoulhon E and Bonazzola S 2002 *Phys. Rev. D* **65** 044020  
Grandclement P, Gourgoulhon E and Bonazzola S 2002 *Phys. Rev. D* **65** 044021  
Cook G 2002 *Phys. Rev. D* **65** 084003
- [30] Shibata M 1999 *Prog. Theor. Phys.* **101** 1199
- [31] Blanchet L 2006 *Liv. Rev. Rel.* **9** 4
- [32] E.g., Akmal A, Pandharipande V R and Ravenhall D G 1998 *Phys. Rev. C* **58** 1804  
Douchin F and Haensel P 2001 *Astron. Astrophys.* **380** 151
- [33] Shibata M and Font J A 2005 *Phys. Rev. D* **72** 047501
- [34] Shibata M and Nakamura T 1995 *Phys. Rev. D* **52** 5428
- [35] Lai D, Rasio F A and Shapiro S L 1993 *Astrophys. J. Suppl.* **88** 205
- [36] Setiawan S, Ruffert M and Janka H-Th 2004 *Mon. Not. R. Astron. Soc.* **352** 753  
Lee W H, Ruiz E R and Page D 2005 *Astrophys. J.* **632** 421
- [37] Shibata M 2003 *Phys. Rev. D* **67** 024033
- [38] E.g., Kidder L, Will C M and Wiseman A G 1993 *Phys. Rev. D* **47** R4183